Sains Malaysiana 54(9)(2025): 2185-2199
http://doi.org/10.17576/jsm-2025-5409-07

Synthesis, Molecular Docking and Dynamic Studies of 3-Cyano-6-Hydroxy-5-Pentaloxy N-Boc Cyclohexene as Key Intermediate for Oseltamivir Phosphate

(Sintesis, Pendokan Molekul dan Dinamik 3-Siano-6-Hidroksi-5-Pentaloksi N-Boc Sikloheksena sebagai Perantara Penting bagi Oseltamivir Fosfat)

ZURHANA MAT HUSSIN[1], NAJMAH P.S HASAN[2], FAZNI SUSILA ABD GHANI[2], SHAARI DAUD[1], MOHD SALLEH ROFIEE[2,3], SYAHRUL IMRAN[2,4] & MOHD TAJUDIN MOHD ALI[2,*]

[1]*Faculty of Applied Sciences, Universiti Teknologi MARA, Cawangan Pahang, 26400 Bandar Tun Abdul Razak, Pahang, Malaysia*
[2]*Faculty of Applied Sciences, Universiti Teknologi MARA, 40450 Shah Alam, Selangor, Malaysia*
[3]*Integrative Pharmacogenomics, Puncak Alam Campus, Universiti Teknologi MARA, 42300 Puncak Alam, Selangor, Malaysia*
[4]*Institute for Natural Product Discovery, Puncak Alam Campus, Universiti Teknologi MARA, 42300 Puncak Alam, Selangor, Malaysia*

Received: 9 April 2025/Accepted: 18 July 2025

ABSTRACT

A key intermediate for oseltamivir phosphate synthesis, compound **15** (3-cyano-6-hydroxy-5-pentaloxy-N-Boccyclohexene), was synthesized from inexpensive, commercially available 1,4-cyclohexadiene (**4**). The synthesis involved eight steps, sequentially introducing substituents onto a cyclohexene ring: An amino group at C1, hydroxy at C6, pentaloxy at C5, and cyano at C3. C1 amination was achieved *via* epoxidation and asymmetric ring opening using a salen complex and $TMSN_3$. The C6 hydroxy group was introduced via one-pot reduction and amine protection. C5 functionalization involved allylic oxidation (SeO_2/TBHP) and etherification with 3-pentanol. The C3 cyano group was formed *via* olefin epoxidation, TMSCN ring opening, and elimination. Molecular docking showed compound **15** had a binding energy of -7.14 kcal/mol, comparable to oseltamivir (-8.5 kcal/mol), suggesting strong neuraminidase binding. A 200 ns molecular dynamics simulation confirmed complex stability, with RMSF analysis indicating stable interactions. The ADMET profile indicates that these compounds exhibit good drug-like properties, including high gastrointestinal (GI) absorption, good solubility, and no inhibition of CYP450 enzymes.

Keywords: Dynamic; epoxidation; neuraminidase; oseltamivir; salen catalyst

ABSTRAK

Sebatian perantaraan utama untuk sintesis oseltamivir fosfat, sebatian **15** (3-siano-6-hidroksi-5-pentaloksi-*N*-Boccyclohexene), telah disintesis daripada 1,4-sikloheksadiena (4) yang murah dan tersedia secara komersial. Sintesis ini melibatkan lapan langkah dengan kumpulan pengganti diperkenalkan secara berurutan ke atas gelang sikloheksena: kumpulan amino pada karbon-1, hidroksi pada karbon-6, pentaloksi pada karbon-5 dan siano pada karbon-3. Penggabungan kumpulan amino pada C1 dicapai melalui tindak balas epoksidasi dan pembukaan gelang tak simetri menggunakan kompleks salen dan $TMSN_3$. Kumpulan hidroksi pada C6 diperkenalkan melalui penurunan satu langkah dan perlindungan amina. Penggantian pada C5 melibatkan pengoksidaan alilik (SeO_2/TBHP) dan eterifikasi dengan 3-pentanol. Kumpulan siano pada C3 dibentuk melalui epoksidasi olefin, pembukaan gelang dengan TMSCN dan tindak balas penyingkiran. Kajian pendokan molekul menunjukkan sebatian **15** mempunyai tenaga pengikatan sebanyak –7.14 kcal/mol, setanding dengan oseltamivir (-8.5 kcal/mol), menunjukkan ikatan yang kuat dengan tapak aktif neuraminidase. Simulasi dinamik molekul selama 200 ns mengesahkan kestabilan kompleks, dengan analisis RMSF menunjukkan interaksi yang stabil. Profil ADMET menunjukkan sebatian-sebatian ini memenuhi ciri ubat yang baik, termasuk penyerapan gastrousus (GI) yang tinggi, keterlarutan yang baik dan tiada perencatan enzim CYP450.

Kata kunci: Dinamik; epoksidasi; mangkin salen; neuraminidase; Oseltamivir

INTRODUCTION

The influenza virus is a highly contagious respiratory pathogen that causes seasonal epidemics worldwide. While infections peak during winter in temperate regions, they can occur year-round in tropical climates (Singh, Gupta & Mishra 2020). Seasonal influenza affects up to

30% of children and 10% of adults globally (WHO 2016), underscoring the ongoing need for effective antiviral therapies. Oseltamivir phosphate 1 (Tamiflu) remains one of the most effective treatments (Kim et al. 1997), functioning as an ethyl ester prodrug that is hydrolyzed into the active neuraminidase inhibitor, oseltamivir carboxylate 2. Its unique alkyl chain and double bond are crucial for binding activity (Davies 2010). Tamiflu is industrially synthesized from (-)-shikimic acid 3, offering synthetic advantages such as a pre-existing double bond and access to key epoxide intermediates (Abrecht et al. 2004; Karpf & Trussardi 2001; Shibasaki, Kanai & Yamatsugu 2011). However, Roche's process poses limitations, including hazardous azide handling and scalability issues (Sagandira & Watts 2020), prompting the development of safer, more efficient synthetic alternatives.

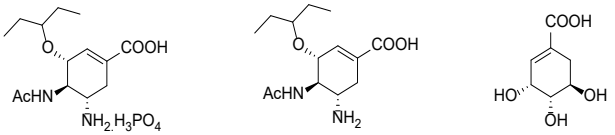

1 2 3

Numerous synthetic routes for oseltamivir phosphate have been reported in the literature, broadly classified into shikimic acid-dependent and shikimic acid-independent approaches. The former relies on azide-based strategies to introduce amino groups onto the chiral cyclohexene ring derived from shikimic acid, as demonstrated in several studies (Sagandira & Watts 2020). In contrast, shikimic acid-independent methods construct the cyclohexene backbone using diverse strategies from both natural and unnatural chiral sources. Notable natural precursors include (–)-quinic acid (Harrington et al. 2004), L-serine (Cong & Yao 2006), D-xylose (Shie et al. 2007), and D-glucose (Zhu et al. 2010). Meanwhile, other synthetic routes involve non-natural starting materials such as Diels–Alder adducts (Yeung, Hong & Corey 2006), Michael addition products (Ishikawa, Suzuki & Hayashi 2009), cyclohexene derivatives (Mita et al. 2007), benzene derivatives (Zutter et al. 2008), Horner–Wadsworth–Emmons products (Chen & Fang 2013), aldol condensation intermediates (Trajkovic, Ferjancic & Saicic 2011), and pyridine derivatives (Satoh et al. 2009). Among these, our study adopts a shikimic acid-independent approach using cyclohexene derivatives from 1,4-cyclohexadiene as the strategic starting material.

In this work, the compound of *tert*-butyl ((1*S*,6*R*)-3-cyano-6-hydroxy-5-(pentan-3-yloxy)cyclohex-3-en-1-yl)carbamate **15** as an intermediate to oseltamivir phosphate *via* proposed sequential reaction steps from 1,4-cyclohexadiene is discussed. The main aim of this study was to establish that key oseltamivir intermediate, *tert*-butyl ((1*S*,6*R*)-3-cyano-6-hydroxy-5-(pentan-3-yloxy) cyclohex-3-en-1-yl)carbamate (**15**), can be practically synthesized via a novel shikimic acid-independent route and that this intermediate is a computationally viable precursor for a potent neuraminidase inhibitor. This work also aims to first establish an accessible synthetic pathway and then computationally validate the resulting intermediate's binding affinity and drug-like properties to confirm its suitability for further development.

The newly synthesized stereoisomer of oseltamivir is expected to exhibit altered interactions within the chiral environment and neuraminidase, potentially leading to distinct antiviral properties. This study presents the development of new synthetic routes for oseltamivir intermediates, utilizing simple, cost-effective, and readily available starting materials. These methods offer a practical and efficient alternative to existing industrial synthesis pathways.

MATERIALS AND METHODS

REAGENTS AND INSTRUMENTATION

All commercial reagents were used as received without further purification. Non-aqueous reactions were conducted under an inert atmosphere of dry nitrogen using glassware dried by heating under reduced pressure. Solvents were purified according to standard procedures where necessary. Column chromatography was performed using Merck 9385 Kieselgel 60-45 (230-400 mesh) and Merck Millipore silica gel 60. Thin-layer chromatography (TLC) was carried out on aluminum-backed plates coated with Merck Kieselgel 60 GF254, and spots were visualized under UV light at 254 nm. Melting points were determined using a Büchi SMP 20 apparatus and are uncorrected. ^{1}H and ^{13}C NMR spectra were recorded on Bruker Avance 400 MHz and 600 MHz spectrometers. IR spectra were obtained using a Bio-Rad Excalibur FTS 3000 spectrometer equipped with a Golden Gate Diamond single reflection ATR system. High-resolution mass spectrometry (HRMS) was performed on an Agilent 6520 LC/MS-QTOF system using a ZORBAX Eclipse Plus C18 column.

SYNTHESIS OF *MESO*-CYCLOHEXADIENE EPOXIDE (5)

Dichloromethane (300 mL) and dipotassium hydrogen phosphate (3.61 g, 20.7 mmol, 1 eq) in 2 mL of water (DCM/H_2O, 150:1) were added to a 1 L round-bottom flask containing 1,4-cyclohexadiene 4 (3.38 g, 42.1 mmol, 1.1 eq) and a magnetic stir bar. The mixture was cooled in an ice bath (0 °C), and m-CPBA (70%, 10.2 g, 41.3 mmol, 1 eq) was added portion wise. The solution was stirred for several hours as it warmed to room temperature, then further stirred for 18 h. The resulting white solid was filtered under vacuum, and the filtrate was washed sequentially with saturated $NaHCO_3$ (2 × 50 mL), 5% Na_2SO_3 (50 mL), water (50 mL), and brine (50 mL). The organic layer was dried over $MgSO_4$ and concentrated under vacuum to yield 3.58 g (89%) of the desired product 6 as a colorless oil, which was then purified by distillation (23 mm Hg, 60 °C).

R_f = 0.23 (hexane/ethyl acetate = 9:1); ^{1}H NMR (300 Hz, $CDCl_3$) δ 5.42 (s, 2H), 3.25 (s, 2H), 2.49 (d, J = 17.6 Hz, 2H), 2.38 (d, J = 17.6 Hz, 2H); ^{13}C NMR (75 Hz, $CDCl_3$) δ 121.3, 50.49, 24.66; IR ν cm^{-1} : 2995, 1665, 1432, 1214, 737.

SYNTHESIS OF (((1*S*,6*S*)-6-AZIDOCYCLOHEX-3-EN-1-YL)OXY)TRIMETHYLSILANE, 7 AND (1*S*,6*S*)-6-AZIDOCYCLOHEX-3-ENOL, 8

The catalyst salen complex **6** (0.437 mg, 0.63 mmol, 2 mol%), was added into 4 mL of dry diethyl ether (Et_2O) containing compound **5** (3.0 g, 31.2 mmol, 1 equiv.) and continuously stirred for 15 min. The mixture was then gradually added with trimethylsilylazide (3.8 mL (ρ = 0.8763 g/cm^3), 32.8 mmol, 1.05 equiv.). The stirring was continued for 46 hours at room temperature, after which the solvent was removed under vacuum to give a yellowish crude product. Purification by the column chromatography on silica gel (hexane/ethyl acetate = 9:1) generated 68% (4.5 g) yield with 85% enantioselectivity of compound **7** (yellowish oil) and 30% (1.29 g) of compound **8** (solid).

Compound **7**, R_f = 0.58 (SiO_2, hexane/ethyl acetate = 9:1); ^{1}H NMR (300 MHz, $CDCl_3$) δ 5.43-5.59 (m, 2H), 3.62-3.72 (m, 1H), 3.42-3.52 (m, 1H), 2.40-2.52 (m, 2H), 2.05-2.10 (m, 1H), 1.93-2.04 (m, 1H), 0.18 (s, 9H); ^{13}C NMR (75 MHz, $CDCl_3$) δ 125.1, 124.3, 76.9, 63.3, 35.1, 31.0, 0.23 (3C); IR ν cm^{-1} : 2916, 2849, 2109, 1436, 1255, 1157, 784.9, 669.1; MS [CI, NH_3] m/z (%) = 212.1 [M + H]$^+$, calculated for [$C_9H_{17}N_3OSi$] : 211.1.

Compound **8**, R_f = 0.41 (SiO_2, hexane/ethyl acetate = 9:1); ^{1}H NMR-Spectra (300 Hz, $CDCl_3$) δ 5.42-5.62 (s, 2H), 3.58-3.80 (m, 1H), 3.32-3.51 (m, 1H), 2.39-2.52 (m, 2H), 1.97-2.15 (m, 2H); ^{13}C NMR-Spectra (75 Hz, $CDCl_3$) δ 124.8, 123.5, 70.1, 63.4, 33.0, 30.2; IR ν cm^{-1} : 3343, 2958, 2906, 1655, 1252, 1108, 668; HRMS [Cl, NH_3]: calculated for [$C_6H_9N_3O$]: 139.076, found, 141.9586 [M + 2H$^+$].

SYNTHESIS OF *TERT*-BUTYL ((1*S*,6*S*)-6-HYDROXYCYCLOHEX-3-EN-1-YL)CARBAMATE, 9 AND *TERT*-BUTYL ((1*S*,6*S*)-6-((TRIMETHYLSILYL)OXY) CYCLOHEX-3-EN-1-YL)CARBAMATE, 10

To a solution of **7** (0.21 g, 1.02 mmol, 1 equiv.) in ethanol (4 mL) was added di-*tert*-butyldicarbonate (Boc_2O; 0.45 g, 2.04 mmol, 2 equiv.), followed by addition of 20% $Pd(OH)_2$/C (10.2 mg) at room temperature. The reaction proceeded with the addition of triethylsilane (0.33 mL, 2.04 mmol, 2 equiv.). After stirring for 24 h, the resulting mixture was filtered through Celite. After complete removal of ethanol, the crude was purified using silica gel column chromatography (pet ether/ethyl acetate =15:0.5) to give **9** (0.23 g, 78%) as a white solid and **10** (0.026 g, 12%) as a yellowish oily substance.

Compound **9**, R_f = 0.25 (SiO_2, hexane/ethyl acetate = 21:7); m.p. 76-78 °C, ^{1}H NMR (300 MHz, $CDCl_3$) δ 5.50-5.60 (m, 2H), 4.90 (brs, 1H), 3.60-3.70 (m, 1H), 3.20-3.30 (m, 1H), 2.30-2.50 (m, 2H), 2.00-2.10 (m, 1H), 1.80-1.90 (m, 1H), 1.43 (s, 9H); ^{13}C NMR (75 MHz, $CDCl_3$) δ 156.9, 124.9, 124.3, 80.1, 70.8, 52.4, 33.9, 31.6, 28.4 (3C); IR ν cm^{-1} : 3376, 3286, 2977, 1674, 1309, 124, 1165, 1071, 871, 852, 742, 660. MS [CI, NH_3] m/z (%) = 213.1 [M$^+$]; Calculated for [$C_{11}H_{19}NO_3$]: 213.14.

Compound **10**, R_f = 0.75 (SiO_2, hexanes/ethyl acetate = 21: 7); ^{1}H NMR (300 MHz, $CDCl_3$) δ 5.55-5.60 (m, 2H), 4.73 (brs, 1H), 3.66-3.72 (m, 1H), 3.27-3.33 (m, 1H), 2.52-2.58 (m, 1H), 2.46-2.48 (m, 1H), 2.12-2.18 (m, 1H), 1.95-2.01 (m, 1H), 1.46 (s, 9H), 0.14 (s, 9H); ^{13}C NMR (75.5 MHz, $CDCl_3$) δ 157.0, 124.9, 124.3, 80.0, 70.9, 52.4, 33.9, 31.6, 28.4 (3C), 0.23 (3C); IR ν cm^{-1} 3340, 2976, 1689, 1366, 1309, 1249, 1170, 1102, 1067, 881, 840, 749, 661. HRMS [Cl, NH_3]: calculated for [$C_{14}H_{27}NO_3Si$]: 285.1760, found 285.1758 [M$^+$].

SYNTHESIS OF *TERT*-BUTYL ((1*S*,6*R*)-5,6-DIHYDROXYCYCLOHEX-3-EN-1-YL)CARBAMATE, 11

The reagent SeO_2 (0.091 g, 0.82 mmol, 1 equiv.) was grounded to a powder form and then added to 3 mL ethanol containing **9** (0.165 g, 0.77 mmol, 1 equiv.). The solution was stirred at room temperature for 10 min. *Tert*-butylhydroperoxide (TBHP, 0.025 mL, 1.4 mmol, 2 equiv.) was added and refluxed for 24 h. The solvent was removed under reduced pressure and the crude product was purified using the silica gel column chromatography (pet ether/ethyl acetate = 27:3) to give 0.1 g (56%) **11** as a white solid. R_f = 0.4 (SiO_2, hexanes/ethyl acetate = 21:7); m.p. 73-75 °C. ^{1}H NMR (300 MHz, $CDCl_3$) δ 5.50-5.90 (m, 2H), 4.43-4.60 (brs, IH), 3.66-3.75 (m, 1H),3.48-3.56 (m, 1H), 3.25-3.44 (m, 1H), 2.35-2.53 (d, J = 15.6, 1H), 1.85-1.95 (d, J = 12, 1H), 1.46 (s, 9H); ^{13}C NMR (75 MHz, $CDCl_3$) δ 156.8, 124.8, 124.3, 79.9, 70.4, 56.5, 52.3, 31.5, 28.4 (3C); IR ν cm^{-1} 3365, 3284, 2972, 1671, 1307, 1246, 1163, 1056, 868, 850, 742, 661. HRMS [Cl, NH_3]: calculated for [$C_{11}H_{19}NO_4$]: 229.1314, found, 252.0994 [M + Na$^+$].

SYNTHESIS OF *TERT*-BUTYL ((1*S*,6*R*)-6-HYDROXY-5-(PENTAN-3-YLOXY)CYCLOHEX-3-EN-1-YL)CARBAMATE (12)

BF_3.OEt_2 (0.09 mL, 2 equiv.) was added dropwise to a solution of compound **11** (0.112 g, 0.49 mmol, 1 equiv.) in 3-pentanol (5 mL), the resulting mixture was stirred at room temperature. After 24 h, saturated aqueous $NaHCO_3$ was added to quench the reaction. The product was extracted with ethyl acetate twice and the combined organic layer was washed with brine and dried over Na_2SO_4. The solvent was removed under pressure and the residue was purified by silica gel column chromatography (pet ether/ethyl acetate = 6:4) to produce **12** (0.08 g, 53%). R_f = 0.69 (SiO_2, hexanes: ethyl acetate 5:5); m.p. 124-126 °C; ^{1}H NMR (300 MHz, CDCl3) δ 5.52-5.62 (m, 2H), 4.58 (brs, 1H), 3.56-3.64 (m, 1H), 3.34-3.45 (m, 1H), 3.15-3.32 (m, 2H), 2.32-2.51 (m, 1H), 1.99-2.09 (m, 1H), 1.81-1.95 (m, 2H), 1.59-

1.67 (m, 2H), 1.45 (s, 9H), 0.81-0.92 (m, 6H); ^{13}C NMR (75 MHz, $CDCl_3$) δ 157.0, 124.9, 124.1, 80.0, 75.6, 71.0, 56.6, 52.4, 31.9, 29.7 (2C), 28.1 (3C), 24.7, 24.0; IR ν cm^{-1} 3373, 3283, 2974, 1675, 1552, 1309, 1247, 1165, 1054, 871, 851, 743, 660; HRMS [Cl, NH_3]: calculated for [$C_{16}H_{29}NO_4$] : 299.2097, found, 324.9000 [M + Na^+ + $2H^+$].

SYNTHESIS OF *TERT*-BUTYL ((3*S*,4*R*)-4-HYDROXY-5-(PENTAN-3-YLOXY)-7-OXABICYCLO[4.1.0]HEPTAN-3-YL) CARBAMATE (13)

Dipotassium hydrogen phosphate (26.129 g, 0.192 mol, 2 equiv.) in 0.2 mL of H_2O was added to a stirred solution of **12** (0.029 g, 0.096 mmol, 1 equiv.) in 5 mL DCM was added at 0 °C. Then *m*-CPBA (70%, 0.049 g, 0.096 mmol, 1 equiv.) was added to the reaction mixture. The white solution was stirred for several hours and the reaction mixture was allowed to warm up to room temperature. The reaction mixture was stirred again for 48 h. Then, an aqueous $Na_2S_2O_3$ solution was added, and the mixture was stirred at room temperature for 1 h. The organic layer was separated, and the aqueous layer was extracted with DCM (2 × 4 mL). The filtrate was washed with 10 mL sat. $NaHCO_3$, 10 mL of NaCl and dried over Na_2SO_4. The crude product was concentrated under vacuum by using rotary evaporator and was purified using silica gel chromatography (pet ether/ethyl acetate = 6:4) to give **13** (0.013 g, 43%) as a white solid. R_f = 0.28 (SiO_2, hexanes/ethyl acetate = 5:5); m.p. 76-78 °C.^{1}H NMR (300 MHz, $CDCl_3$) δ 5.1 (brs, IH), 3.63-3.79 (m, 2H), 3.16-3.31 (m, 2H), 2.31-2.47 (m, 2H), 2.15-2.24 (m, 1H), 1.64-1.98 (m, 4H), 1.50 (m, 6H), 1.45 (s, 9H); ^{13}C NMR (75 MHz, $CDCl_3$) δ 156.1, 79.8, 66.1, 51.8, 51.3, 49.4, 31.6, 29.6 (2C), 28.4 (3C), 26.9 (2C); IR ν cm^{-1} 3458, 2942, 1737, 1460, 1300, 1233, 1097, 1043, 917, 847, 786, 634; HRMS [Cl, NH_3]: calculated for [$C_{16}H_{29}NO_5$]: 315.2046, found 317.2075 [M + $2H^+$].

SYNTHESIS OF *TERT*-BUTYL ((1*S*,2*R*)-5-CYANO-2,4-DIHYDROXY-3-(PENTAN-3-YLOXY)CYCLOHEXYL) CARBAMATE (14)

To a solution of the compound **13** (0.014 g, 0.04 mmol, 1 equiv.) and $LaCl_3.7H_2O$ (0.016 g, 0.04 mmol, 1equiv.) in DCM (4 mL) was gradually added TMSCN (0.006 mL, 0.04 mmol, 1 equiv.) at room temperature. The mixture was stirred for 24 h. After completion of the reaction, the reaction mixture was extracted with diethyl ether, dried over anhydrous Na_2SO_4 and concentrated using rotary evaporator. The crude product was purified by column chromatography using 7:3 (hexane:ethyl acetate) to afford **14** (0.006 g, 49%). R_f = 0.28 (SiO_2, hexanes/ethyl acetate = 5:5); m.p. 76-78 °C; ^{1}H NMR (300 MHz, $CDCl_3$) δ 4.01-4.08 (t, *J* = 5.6, 5.5 Hz, 1H), 3.59-3.67 (m, 1H), 3.41-3.43 (m, 3H), 2.45-2.55 (m, 1H), 2.29-2.35 (t, *J* = 8.0, 7.1 Hz, 1H), 2.05-2.11 (m, 1H), 1.63-1.67 (m, 4H), 1.27 (S, 9H), 0.78-0.89 (m, 6H); ^{13}C NMR (75 MHz, $CDCl_3$) δ 146.5, 129.0, 97.6, 80.3, 70.0, 64.4, 62.8, 59.7, 51.2, 41.6, 32.0, 29.7, 26.5, 14.2; HRMS [Cl, NH_3]: calculated for [$C_{17}H_{30}N_2O_5$]: 342.2155, found, 343.2999 [M + H^+].

SYNTHESIS OF *TERT*-BUTYL (1*S*,6*R*)-3-CYANO-6-HYDROXY-5-(PENTAN-3-YLOXY)CYCLOHEX-3-EN-1-YL)CARBAMATE (15)

Trifluoromethanesulfonic anhydride (5 μL, 0.05 μmol) carbamate was added to a stirred solution of **14** (0.02 g, 0.06 mmol, 1 equiv.) in 5 mL dry THF at 0 °C. The reaction was stirred for 8 hours under N_2 atmosphere. The reaction mixture was concentrated using rotary evaporator under reduced pressure to give brownish crude product, which was purified by column chromatography on silica gel (hexane/ethyl acetate = 7:3) to furnish 0.007 g (41%) of **15**. R_f = 0.37 (SiO_2, hexanes/ethyl acetate = 5:5); ^{1}H NMR (300 MHz, $CDCl_3$) δ 5.76-5.78 (dd, *J* = 2.4, 3.0 Hz, 1H), 3.97-4.00 (m, 2H), 3.47-3.50 (m, 2H), 2.37-2.41 (t, *J* = 3.98, 8 Hz, 1H), 2.02-2.08 (m, 1H), 1.80-1.87 (m, 2H),1.47-1.50 (m, 2H), 1.27 (s, 9H), 0.75-0.86 (m, 6H); ^{13}C NMR (75 MHz, $CDCl_3$) δ 154.8, 145.9, 126.3, 82.6, 70.7, 66.1, 61.8, 49.6, 32.0, 29.5, 26.6, 22.8, 14.2; HRMS [Cl, NH_3]: calculated for [$C_{17}H_{28}N_2O_4$]: 324.2049, found, 325.2905 [M + H^+].

MOLECULAR DOCKING STUDIES

The 3D structure of neuraminidase in complex with oseltamivir (PDB ID: 5L15) was retrieved from the Protein Data Bank and processed using AutoDockTools (ADT) v1.5.6. Water molecules, non-essential heteroatoms, and the co-crystallized ligand were removed, while polar hydrogens and Gasteiger charges were added. To validate the docking protocol, the extracted oseltamivir ligand was redocked into the prepared receptor. The receptor was then saved in PDBQT format. The docking grid was set using AutoGrid to cover the active site (x = 26.5, y = -17.5, z = -63.0), with a spacing of 0.375 Å. Test ligands (11-15) were drawn using ChemDraw, optimized using the MMFF94 force field, and converted to PDBQT format in ADT after defining torsional bonds and assigning charges. Molecular docking was performed using AutoDock 4.2 with the Lamarckian Genetic Algorithm (LGA).

MOLECULAR DYNAMICS

Molecular dynamics (MD) simulations were conducted using Desmond (Schrödinger Suite) to assess the stability of ligand-bound neuraminidase (PDB ID: 5L15). The complex was solvated in a TIP3P water box (10 Å buffer), neutralized with Na^+/Cl^- ions, and supplemented with 0.15 M NaCl to mimic physiological conditions. System preparation used the OPLS4 force field with the default relaxation protocol. Simulations were run for 200 ns under NPT conditions (300 K, 1 atm) using the Nose–Hoover thermostat and Martyna–Tobias–Klein barostat. PME was applied for long-range electrostatics, with a 9 Å cutoff

for van der Waals interactions. Trajectories were saved every 10 ps and analysed for RMSD, RMSF, Rg, hydrogen bonding, and ligand stability using Maestro's Simulation Interaction Diagram tool.

IN SILICO ADME

Pharmacokinetic and drug-likeness properties were predicted using SwissADME (http://www.swissadme.ch/). Ligands were converted to SMILES format via ChemDraw and uploaded for analysis. Key parameters assessed included lipophilicity (LogP), solubility, GI absorption, BBB permeability, CYP450 inhibition, and drug-likeness (Lipinski's rules). Medicinal chemistry filters (PAINS and Brenk alerts) were used to flag potential reactivity or toxicity.

RESULTS AND DISCUSSION

SYNTHESIS OF 3-CYANO-6-HYDROXY-5-PENTALOXY-*N*BOCCYCLOHEXENE OR *TERT*-BUTYL ((1*S*,6*R*)-3-CYANO-6-HYDROXY-5-(PENTAN-3-YLOXY)CYCLOHEX-3-EN-1-YL) CARBAMATE

To address the hypothesis, the primary focus is on the synthetic challenge. The overall strategy involved an eight-step synthesis starting from inexpensive 1,4-cyclohexadiene (**4**) to construct the key intermediate **15** using starting material, 1,4-cyclohexadiene **4** which offers numerous opportunities to incorporate diverse functional groups on both the vinylic and allylic positions surrounding its subunit. To develop the epoxide, the vinylic site of 1,4-cyclohexadiene **4** was oxidized using *m*-CPBA as the oxygen donor. Based on Perlman and Albeck's method (2000), epoxidation in the presence of KH_2PO_4 yielded meso-cyclohexadiene epoxide **5** as the major product (89%) and a minor diepoxide (8%). To construct *N*-substituted compounds with two vicinal stereogenic centers, the asymmetric ring-opening (ARO) approach by Martínez et al. (1995) was applied. This method used 2 mol% of (*R*,*R*)-(salen)Cr(III)Cl complex **6** and trimethylsilylazide ($TMSN_3$) to open the epoxide ring of compound **5**, producing (((1S,6S)-6-azidocyclohex-3-en-1-yl)oxy)trimethylsilane **7** in 68% yield with 85% ee, and (1*S*,6*S*)-6-azidocyclohex-3-enol 8 in 30% yield. The proposed mechanism for asymmetric ring opening of *meso*-cyclohexadiene epoxide **5** catalyzed by **6a** was referring to the study by Hansen, Leighton and Jacobsen in 1996. In the mechanism of asymmetric nucleophilic ring-opening of epoxides catalyzed by (Salen)Cr(III) complexes, the active catalyst was characterized, identified of initially formed intermediate in the ring-opening reaction, and compelling kinetic and structural evidence that this transformation proceeds via catalyst activation of both the nucleophile and the electrophile in a bimetallic enantioselectivity-determining step.

Based on their findings, we proposed that in the initial stages of the ARO reaction of compound **5** with **6a,** there was the formation of chloride-epoxide addition products (**6a**) in amounts according to the catalyst loading. The azide complex **5b** was demonstrated to possess catalytic activity in the ARO process and exhibit recyclability. This suggests that compound **6a** functions as a precatalyst in the reaction. Based on Hansen, Leighton and Jacobsen's group (1996) kinetic studies, the proposed reaction rate is dependent on the concentration of **5b** in a second-order manner, while it will be independent of the concentration of the azide source. Furthermore, the reaction rate exhibits an inverse-order dependence on the concentration of the epoxide. The effective use of $TMSN_3$ necessitated the presence of a minimal quantity of water to generate a catalytic quantity of HN_3, the compound responsible for facilitating turnover. The resulting alkoxide intermediate **5d** will undergo a rapid reaction with HN_3 to afford azido alcohol **8** and regenerate catalyst **6b**. At the same time, catalytic reactions were carried out with $TMSN_3$ to afford compound **7** (Scheme 1).

Following the one-pot method by Kotsuki, Ohishi and Araki (1997) and Ali, Husin and Macabeo (2001), compound **7** underwent azide reduction and *in situ* amine protection via hydrogenation using $Pd(OH)_2/C$ and trapping with di-tert-butyl dicarbonate in ethanol, followed by triethylsilane as a proton donor. Ethanol was selected as the reaction medium due to its suitability for reductive amination. This yielded *tert*-butyl ((1*S*,6*S*)-6-hydroxycyclohex-3-en-1-yl)carbamate **9** in 78% and *tert*-butyl ((1*S*,6*S*)-6-((trimethylsilyl)oxy)cyclohex-3-en-1-yl) carbamate **10** in 12%.

Allylic oxidation at activated positions can selectively yield desired products, with outcomes depending on reagent type and reaction conditions. In this procedure, selenium dioxide was added to a solution of *tert*-butyl ((1*S*,6*S*)-6-hydroxycyclohex-3-en-1-yl)carbamate **9** in ethanol, followed by *tert*-butyl hydroperoxide (TBHP). TBHP was introduced at a later stage to enhance selectivity, as its *tert*-butylperoxy radical can abstract hydrogen from an activated site with minimal energy input (Blanksby & Ellison 2003). The bulky *N*-Boc group at C-1 hindered hydrogen abstraction at C-2, and the [2,3]-sigmatropic rearrangement was favoured at the less hindered side (Murphy, Mallat & Baiker 2000). Consequently, hydroxylation at C-5 was achieved, yielding racemic *tert*-butyl((1*S*,6*R*)-5,6-dihydroxycyclohex-3-en-1-yl) carbamate **11** in 56%. To add the target pentaloxy group at C-5, compound **11** was treated with 3-pentanol and $BF{\cdot}OEt_2$ via etherification to form *tert*-butyl ((1*S*,6*R*)-6-hydroxy-5-(pentan-3-yloxy)cyclohex-3-en-1-yl)carbamate **12** (53%). The second epoxidation step, key for introducing two new contiguous stereocentres at C-3 and C-4, involved converting compound **12** into epoxide **13** using reagents a–d (Scheme 2). As summarized in Table 1, the reaction was conducted between 0°C and room temperature under varied solvents and durations.

The desired product was obtained in 43% yield as a racemic mixture. Polar aprotic solvent such as DCM with 9.1 dielectric constant is an efficient solvent for epoxidation when used with *m*-CPBA where free ions are not involved in the reaction. The asymmetric ring opening of epoxide was again applied in this reaction steps but now using TMSCN in the presence of Lewis acid $LaCl_3.7H_2O$ as its reagent. This reaction was produced *tert*-butyl ((1*S*,6*R*)-3-cyano-4,6-dihydroxy-5-(pentan-3-xyloxy)cyclohexan-1-yl)carbamate **14** in 49% yield. Reduction of OH group at carbon-4 after treatment with TF_2O in a polar aprotic solvent, THF at 0 °C gave 41% of *tert*-butyl(1*S*,6*R*)-3-cyano-6-hydroxy-5-(pentan-3-yloxy)cyclohex-3-en-1-yl) carbamate **15**. The hydroxyl group on carbon-4 or near to nitrile group in cyclohexanenitrile **14** should be eliminated rather than hydroxy on the carbon-6 to get the target product due to its less steric hindrance. The overall steps in the synthesis of oseltamivir phosphate intermediate are shown in Scheme 3.

MOLECULAR DOCKING STUDIES

Following the successful synthesis of intermediate **15** and its precursors, the compounds were computationally evaluated for their potential as neuraminidase inhibitors. Molecular docking and dynamics simulations were conducted to assess binding affinity and stability within the active site. Docking validation was performed by re-docking oseltamivir into neuraminidase (PDB ID: 5L15), yielding an RMSD of 0.73 Å, confirming the reliability of the protocol (Figure 1). Docking was carried out using AutoDock 4.2 with an empirical scoring function incorporating van der Waals forces, hydrogen bonding, electrostatics, desolvation, and torsional entropy. More negative binding energies indicate stronger predicted affinity. The best binding pose for each compound was selected based on binding energy and key interactions with catalytic residues (Arg294, Arg372, Glu278), supporting their potential inhibitory activity. Compounds **11-15**, which have similar structure to oseltamivir, were subjected through docking to identify how each of these compounds could plausibly bind within the neuraminidase active site. The molecular docking results provide insights into the binding affinities of Oseltamivir and compounds **11-15** to the target protein (Table 2). Oseltamivir exhibits the lowest binding energy (-8.50 kcal/mol), signifying the strongest binding affinity among the tested molecules. This suggests that Oseltamivir forms highly stable interactions with the target protein, likely through a combination of hydrogen bonding, hydrophobic interactions, and electrostatic forces. Among the test compounds, compound **13** (-7.23 kcal/mol) and compound **15** (-7.14 kcal/mol) demonstrate the

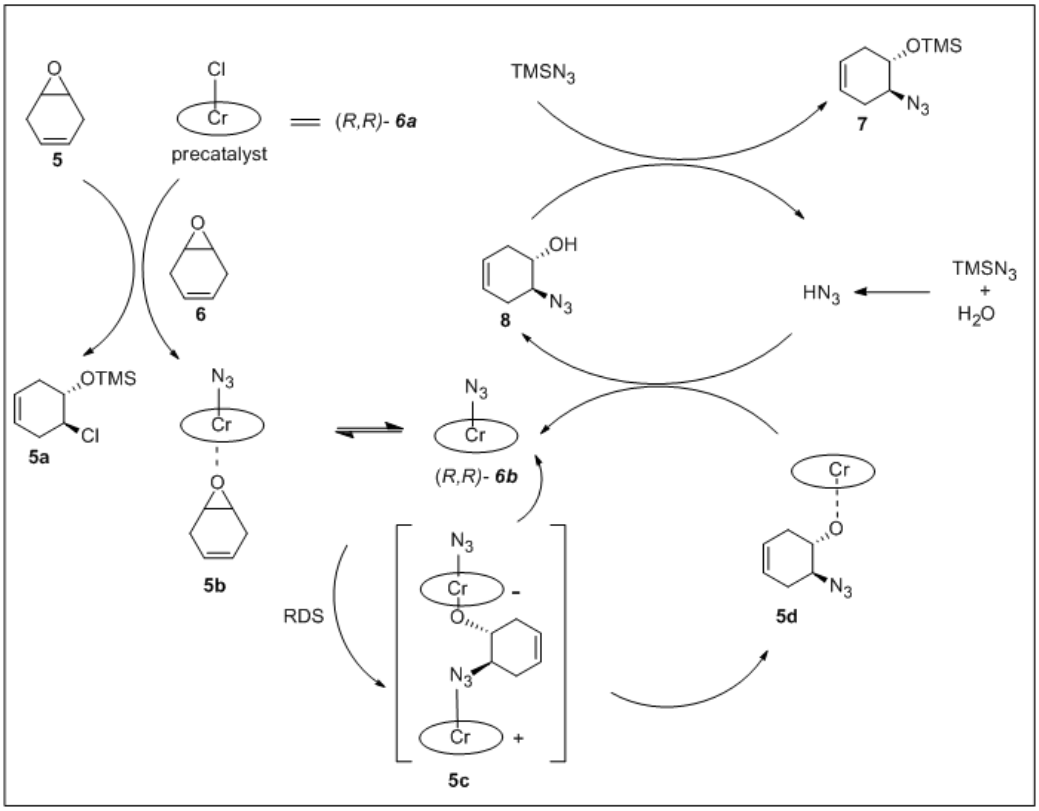

SCHEME 1. The proposed catalytic cycle of *meso*-cyclohexadiene epoxide catalyzed by Salen complexes

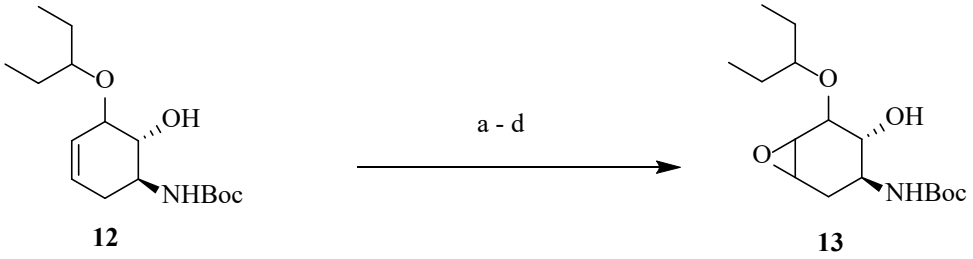

SCHEME 2. Variable conditions of epoxidation of *N*-Boc pentaloxy **12**. Reagent and conditions: *m*-CPBA, K_2HPO_4, solvent, time as stated in Table 1(a-d), 0 °C to r.t

TABLE 1. Epoxidation of *N*-Boc Petaneyloxy **12** in variables type solvent and time

	Reaction conditions	Solvent	Time (h)	Product 13 (%)
a	*m*-CPBA (1.5 eq), K_2HPO_4 (2 equiv)	EtOH	24	trace
b	*m*-CPBA (2 eq), K_2HPO_4 (2 equiv)	THF	24	trace
c	*m*-CPBA (2 eq), K_2HPO_4 (2 equiv)	EtOH (50%)	24	19
d	*m*-CPBA (2 eq), K_2HPO_4 (2 equiv)	DCM (50%)	48	43

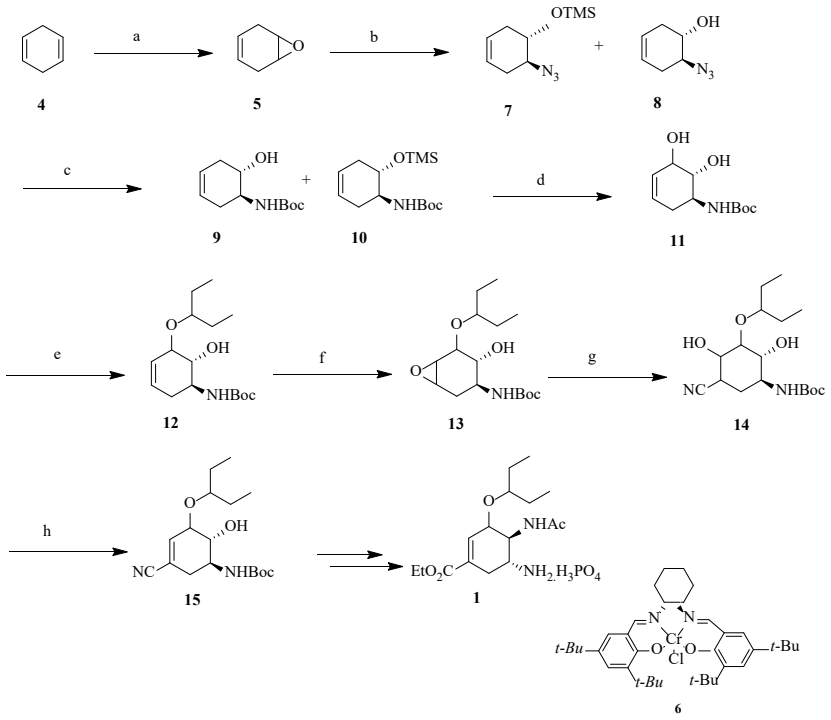

SCHEME 3. Synthesis towards the target molecule, oseltamivir phosphate **1**. Reagent and conditions: (a) *m*-CPBA (1 equiv.), K_2HPO_4 (1 equiv.), DCM, 0 °C, 20 h, 89%. (b) Salen complex **6**, $TMSN_3$, Et_2O, 46 h, r.t, 68% with 85% ee of **7** and 47% of **8**. (c) Boc_2O, $Pd(OH)_2/C$, EtOH, 18 h, r.t, 78% of **9** and 12% of **10**. (d) SeO_2, TBHP, EtOH, 24 h, r.t, 56% of **11**. (e) BF_3OEt_2, 3-pentanol, 24 h, r.t, 53% of **12**. (f) *m*-CPBA, K_2HPO_4, DCM, 0 °C to r.t, 48 h, 43% **13**. (g) TMSCN, $LaCl_3.7H_2O$, DCM, r.t, 24 h, 49% **14** (h) TF_2O, THF, 0 °C, 8 h, r.t, 41% of **15**

closest binding affinities to Oseltamivir, suggesting their potential as effective alternatives. Their strong binding suggests that they may adopt similar binding poses and interaction patterns within the active site. On the other hand, compounds **11** (-2.82 kcal/mol) and **12** (-4.75 kcal/mol) exhibit significantly weaker binding, indicating lower interaction stability and potential reduced inhibitory potency. The relatively higher binding energy values suggest that these compounds may lack critical binding interactions or experience steric hindrance, leading to suboptimal docking poses. Compound **14** (-4.89 kcal/mol) also demonstrates moderate binding affinity, but it does not perform as well as compounds **13** and **15** in terms of docking energy.

Compound **11** interacts with neuraminidase via three key hydrogen bonds and several van der Waals and hydrophobic contacts (Figure 2). The benzylic hydroxyl forms a strong hydrogen bond with Arg153 (1.94 Å) and a secondary interaction at 3.06 Å, while a longer-range polar contact with Arg294 (5.67 Å) suggests potential for optimization. Additional van der Waals interactions with Glu278, Asn296, and Arg226, along with hydrophobic contacts involving Leu135 and Ile224, help stabilize the ligand. The phenolic hydroxyl and benzylic hydroxyl are critical for hydrogen bonding and polarity, while the NH–Boc carbamate contributes steric and polar support. SAR analysis highlights the importance of these functional groups, and enhancing interactions with Arg294 or refining the benzylic hydroxyl orientation may improve binding. Compound **12** similarly forms three hydrogen bonds, with a strong interaction between the cyclohexenyl hydroxyl and Tyr406 (2.19 Å), a key catalytic residue. Weaker hydrogen bonds with Arg119 and Arg372, along with hydrophobic interactions via the ethoxypropyl chain and contacts with Ala248, Glu278, Asn296, and Ile224, support ligand binding. The NH–Boc carbamate and aromatic ring also contribute to binding through polar and hydrophobic interactions. While it lacks strong contact with Arg294, its Tyr406 interaction may compensate. SAR analysis points to the hydroxyl, ether, and aromatic regions as key contributors, and further optimization of these groups could enhance inhibitory activity.

As for compound **13**, it forms strong hydrogen bonds with Glu120 (2.03 Å) and Glu229 (2.47 Å) via its secondary hydroxyl and cyclic ether groups, anchoring it firmly in the active site. A weaker interaction with Arg119 (5.24 Å) and a C–H bond with Ser181 (2.92 Å) further orient the ligand. Van der Waals interactions with Trp180, Tyr406, Ile224, and Glu278 are stabilized by the ether-linked side chain and aromatic ring, with possible π–π stacking involving Trp180. A hydrophobic interaction with Ala248 (4.17 Å) via the isopropyl ether moiety enhances anchoring. These findings suggest that compound **13** benefits from a balanced polar and nonpolar interaction profile, with optimization possible through improved Arg119 alignment or alkyl chain extension. Compound **14**, a hydroxynitrile analog of **13**, exhibits stronger binding through an extended hydrogen bond network involving Arg153, Arg372, Arg294, and Glu279. The hydroxyl and nitrile substituents increase donor/acceptor capabilities without adding steric hindrance, improving insertion into the catalytic pocket. Additional van der Waals interactions with Glu278, Arg226, Ile224, Thr227, and Ala248 support both hydrophobic fit and spatial complementarity. SAR suggests that the polar–nonpolar balance in compound **14** mimics substrate binding well, and minor modifications to the nitrile or alkyl tail could enhance potency further. On the other hand, compound **15** shows a weaker binding profile, with a long hydrogen bond to Arg372 (6.25 Å) and no direct engagement of the nitrile group, indicating suboptimal polar interaction. A hydrophobic interaction with Ala248 (3.60 Å) via the isopropyl ether contributes to nonpolar anchoring, while van der Waals contacts with Ile224, Arg226, Glu278, and Asn296 offer modest support. Despite containing key pharmacophores (hydroxyl, nitrile, ether, carbamate), compound **15** lacks effective electrostatic engagement. Repositioning the nitrile and refining the alkyl chain may improve its overall binding efficiency.

MOLECULAR DYNAMICS

Molecular dynamics (MD) simulations were conducted over 200 ns to evaluate the structural stability of Oseltamivir and test compounds **11**-**15** in complex with neuraminidase (Figure 3). Root mean square deviation (RMSD) was used to assess conformational fluctuations of each ligand, where lower RMSD values indicate higher binding stability. Oseltamivir, the reference drug, exhibited excellent stability with an average RMSD of 3.13 Å (SD = 0.09 Å), remaining within 2.86-3.15 Å during the final 20 ns. This consistency reflects strong retention within the active site and supports its known potency as a neuraminidase inhibitor. Among the test compounds, compound **11** showed the greatest instability, with an average RMSD of 28.33 Å and a fluctuating range of 23.67-27.24 Å in the final phase, indicating poor binding retention and possible detachment from the active site. Compound **12** exhibited moderate instability, with an average RMSD of 16.90 Å, suggesting weak ligand–protein interactions due to conformational flexibility. In contrast, compounds **13**, **14**, and **15** demonstrated strong binding stability. Compound **13** had an average RMSD of 3.18 Å (SD = 0.09 Å), closely mirroring oseltamivir, indicating firm anchoring within the pocket. Compound **15** also showed stable behaviour, with RMSD values between 2.95-3.09 Å and an average of 3.15 Å during the final phase. Remarkably, compound **14** displayed the lowest RMSD (avg. 2.68 Å; SD = 0.07 Å), indicating the most stable ligand–protein conformation among all candidates. Overall, the RMSD profiles rank compound **14** as the most stable, followed by compounds **13** and **15**, whose profiles are comparable to oseltamivir.

TABLE 2. Binding energies of Oseltamivir and Compounds **11-15** against Neuraminidase enzyme

Compound	Energy (Kcal/mol)
11	-2.82
12	-4.75
13	-7.23
14	-4.89
15	-7.14
Oseltamivir	-8.50

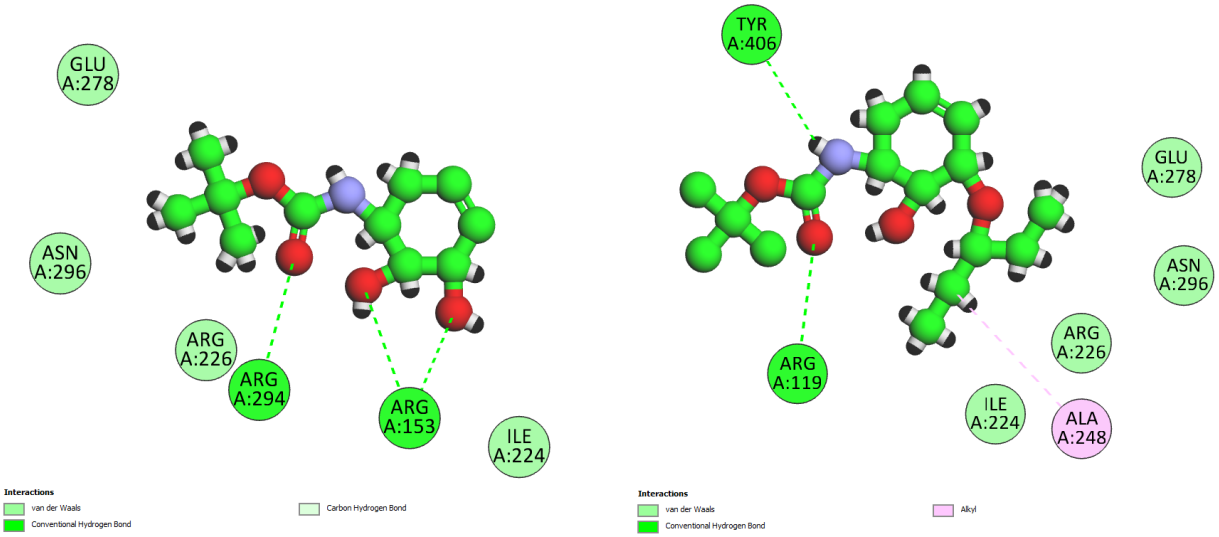

FIGURE 1. Binding position of compounds **11** and **12** within the active site of neuraminidase

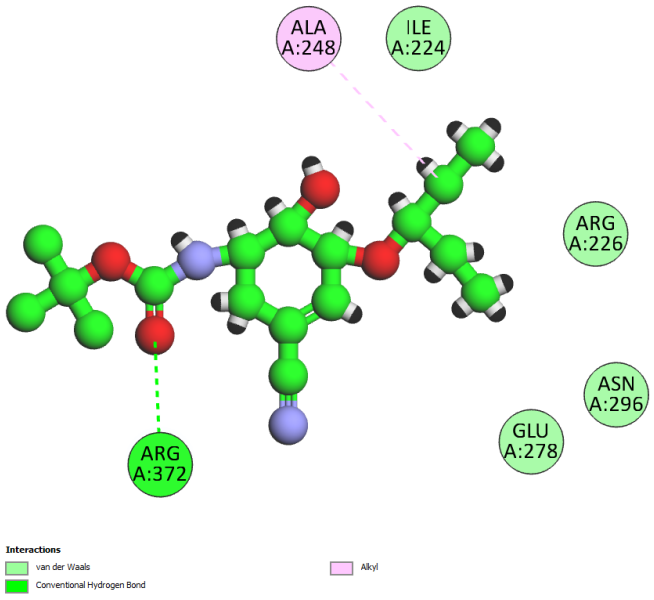

FIGURE 2. Molecular docking of compounds **13**, **14**, and **15** within the active site of neuraminidase

Compound **12** displayed moderate deviations, while compound **11** showed extensive fluctuations, suggesting weak or unstable binding. These results align with docking observations and further support compound **14** as a promising neuraminidase inhibitor.

Root Mean Square Fluctuation (RMSF) analysis was used to assess residue-level flexibility of neuraminidase over a 200 ns MD simulation with oseltamivir and compounds **11-15** (Figure 4). RMSF values reflect the mobility of Cα atoms, where lower values indicate stable, well-anchored regions critical for strong ligand binding. Oseltamivir exhibited consistently low RMSF values across the active site, reflecting strong binding and structural rigidity ideal for effective inhibition. In contrast, compounds **11** and **12** showed elevated fluctuations at key catalytic residues including Arg83, Asn84, Glu111–Ser113, Gly143, Ile150, and Asp152, indicating poor stabilization and weak active-site engagement. Additional flexibility at loop regions (e.g., Glu467, Leu470) further supports potential structural destabilization. Compounds **13**, **14**, and **15** demonstrated more favourable profiles, with reduced fluctuations at residues such as Asp152, Glu231, Tyr468, and Trp208. Notably, compound **15** induced the lowest RMSF values at core catalytic residues, closely matching oseltamivir's profile. It also suppressed flexibility at Arg174, Tyr209, and Phe243, suggesting a conformationally stable binding mode. Overall, RMSF results highlight oseltamivir as the most stabilizing ligand, with compound **15** emerging as a promising analog. Compounds **13** and **14** showed moderate stability, while compounds **11** and **12** exhibited excessive flexibility, indicating suboptimal binding. These findings support prioritization of compound **15** for further development and experimental validation.

RMSF analysis of oseltamivir and compounds **11-15** offers key insights into their conformational flexibility and structural stability during the 200 ns simulation (Figure 5). Oseltamivir showed moderate RMSF values (1.47–11.1 Å), with peaks at atoms 2 and 18, suggesting localized motion possibly due to solvent exposure or flexible functional groups. While some flexibility aids binding adaptability, excessive fluctuations may weaken ligand retention. Compound **11** displayed slightly higher RMSF values (up to 16.46 Å), particularly at atoms 14-16, indicating localized flexibility that could impact binding conformation. Compound **12** exhibited the highest structural fluctuations, with multiple regions exceeding 20 Å, highlighting poor rigidity and potential binding instability. In contrast, compound **13** showed relatively low RMSF values (<5 Å) across most atoms, except for atoms 19-21 (~14 Å), suggesting good overall structural stability with some terminal flexibility. Compound **14** demonstrated the lowest and most uniform RMSF profile (<12.3 Å), with limited fluctuations at atoms 22-24, reflecting strong conformational rigidity likely to support stable protein-ligand binding. Compound **15** also maintained a stable core structure, with atoms 1-13 showing very low fluctuations (<0.4 Å). However, peripheral atoms (14-17, 19-23) exhibited moderate flexibility (~1.45 Å), likely due to solvent exposure. This balance of a rigid core and adaptable side groups may support both stable binding and conformational fit. Compound **14** emerges as the most stable ligand, followed by compounds **13** and **15**. Compound **12** shows excessive flexibility, indicating weaker stability. Oseltamivir and compound **11** exhibit moderate fluctuation profiles, suggesting a compromise between rigidity and adaptability. These findings support prioritizing compound **14** for further development based on its favourable dynamic behaviour.

The ligand–protein interaction analysis over a 200 ns MD simulation highlights only interactions persisting above 30% of the time (Figure 6). Oseltamivir forms strong, consistent hydrogen bonds and electrostatic contacts with Arg152 (98%), Arg294 (100%), Glu120 (99%), and Asp152 (90%), indicating tight active-site retention. Compound **11** shows limited interaction, with few contacts exceeding 30%. The lack of engagement with Arg152 and Arg294 reflects poor stabilization within the active site. Compound **12** exhibits similarly weak interaction, with minimal hydrogen bonding and greater solvent exposure, suggesting reduced binding strength. Compound **13** forms frequent hydrogen bonds with Arg152, Glu120, and Asp152, reaching up to 90% occupancy. Hydrophobic and polar interactions contribute to a stable complex with enhanced binding. Compound **14** maintains persistent hydrogen bonding with Arg153 (2.18 Å), Arg294 (2.87 Å), Arg372 (2.67 Å), and Glu279 (2.31 Å). These contacts, supported by van der Waals interactions with Glu278, Arg226, Ile224, and Thr227, stabilize the ligand within both polar and nonpolar regions of the binding pocket. Compound **15** engages Arg372 via direct hydrogen bonding (55%) and Arg294 through a water-mediated interaction (44%). Asp152 maintains hydrogen bonding for 70% of the simulation. Tyr406 forms stable hydrophobic contact for 98% of the simulation, and the ester group shows an exceptionally high interaction frequency (139%), suggesting overlapping or repeated interactions. Compound **14** exhibits a similar interaction profile, maintaining key charged residue interactions, which could enhance its inhibitory potential. These findings are consistent with docking predictions for compound **15**, which identified residue Arg372 as a key hydrogen bonding partner and Ala248 as a hydrophobic anchor point. The MD analysis confirms the Arg372 interaction (55% occupancy) and further shows water-mediated contacts with Arg294 (44%) and Asp152 (70%), which were not observed in the docking pose. In addition to that, the strong hydrophobic interaction with Tyr406 (98%) and high interaction frequency of the ester group (139%) highlighted on the significance of nonpolar contacts in ligand stabilization. While docking initially suggested moderate binding, the dynamic profile highlights a more favourable binding environment for compound **15**, supported by both

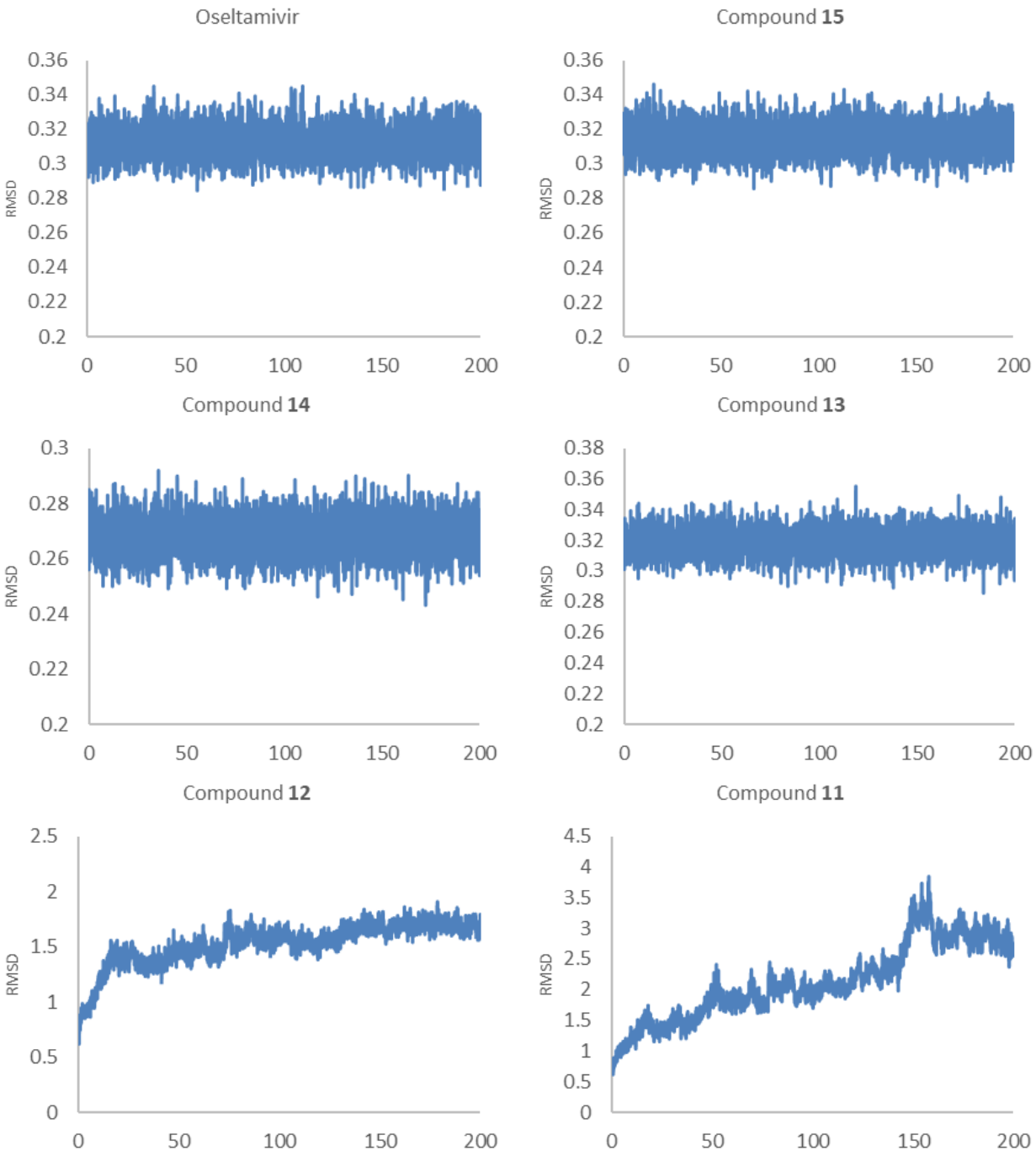

FIGURE 3. RMSD plot for compounds **11-15** and Oseltamivir

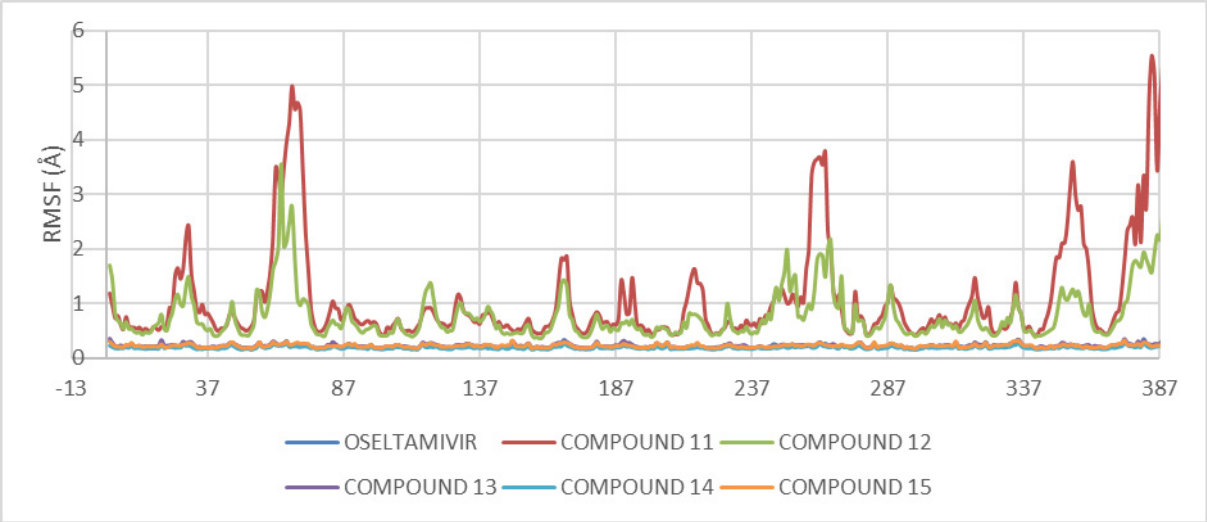

FIGURE 4. RMSF of individual neuraminidase protein residues

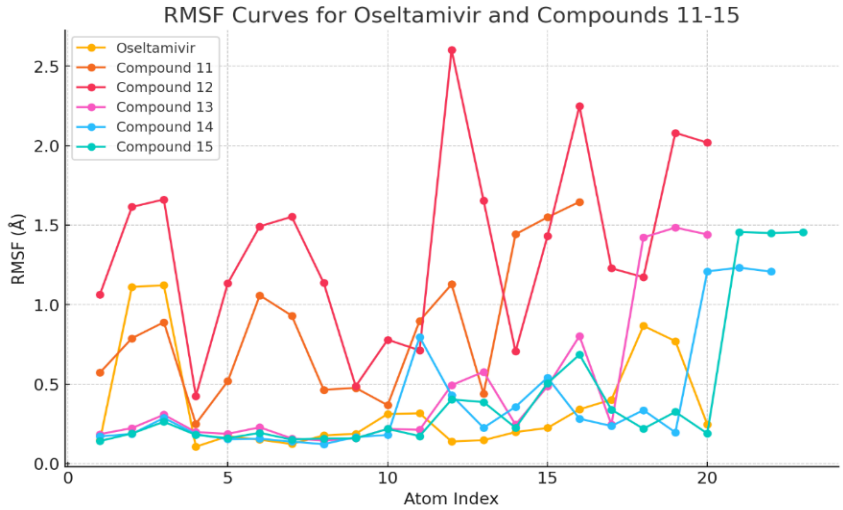

FIGURE 5. RMSF of individual atoms for compounds **11-15** and oseltamivir

electrostatic and hydrophobic contributions. Overall, the most stable interactions are observed in Oseltamivir, compounds **13**, **14**, and **15** which maintain multiple hydrogen bonds and electrostatic contacts throughout the simulation. Compounds **11** and **12** appear to be the least stable, potentially due to weak interactions and increased solvent exposure.

in silico ADMET ANALYSIS

The SwissADME evaluation of compounds **11-15** highlights key ADMET properties relevant to drug-likeness and pharmacokinetics (Table 3). All compounds comply with Lipinski's Rule of Five, with molecular weights ranging from 229.27 to 342.43 Da, logP values between 0.57 and 2.69, and TPSA values below 140 Å², suggesting good absorption and membrane permeability. All compounds exhibit high gastrointestinal (GI) absorption, supporting oral bioavailability. Compound **11** is classified as very soluble, while compounds **12-15** are soluble. None are predicted to cross the blood-brain barrier (BBB), minimizing potential CNS side effects. Only compound **14** is a predicted P-glycoprotein (P-gp) substrate, indicating possible cellular efflux and reduced bioavailability; the rest are not P-gp substrates. Metabolic predictions show no inhibition of major CYP450 isoforms (CYP1A2, 2C19, 2C9, 2D6, 3A4), reducing the risk of metabolic interactions or hepatic toxicity. All compounds have balanced excretion

Oseltamivir

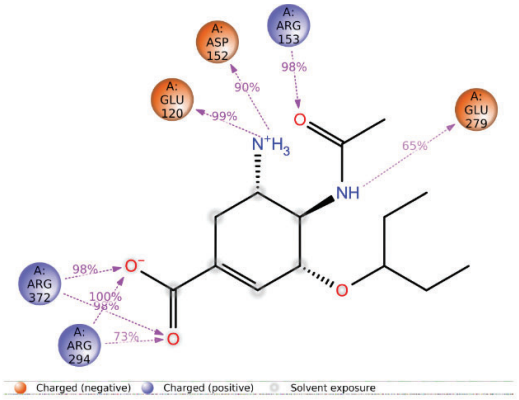

Compound **15**

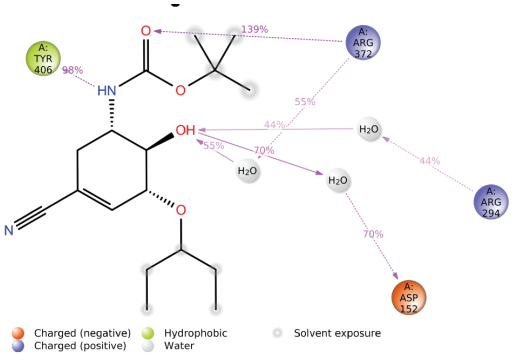

Compound **14**

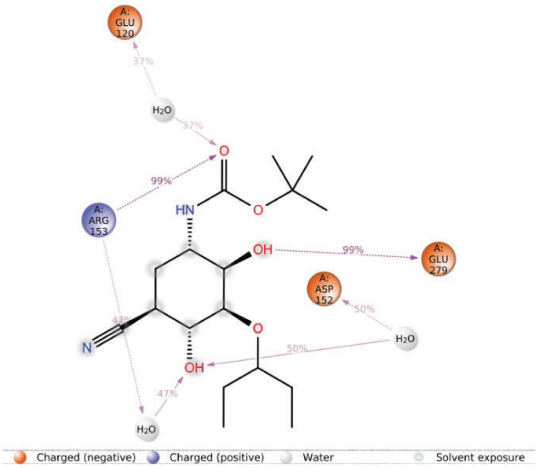

Compound **13**

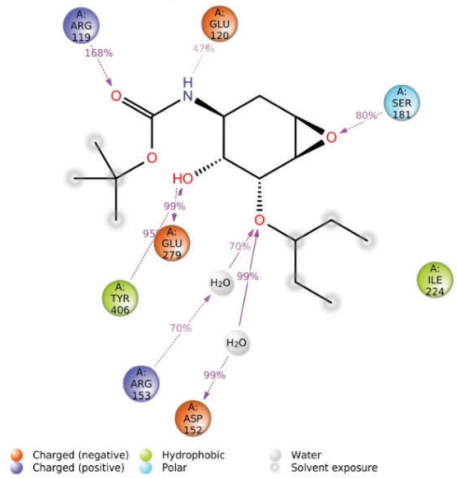

Compound **12**

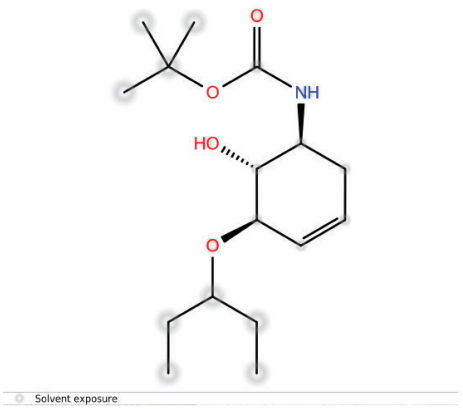

Compound **11**

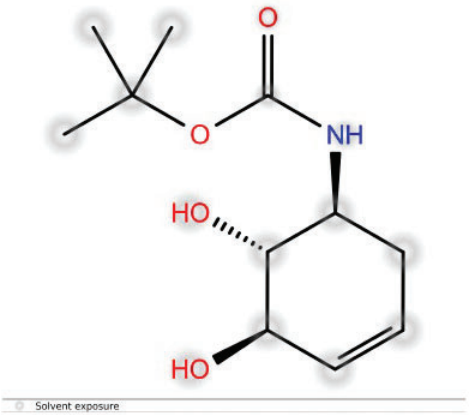

FIGURE 6. Binding interaction for compounds **11**-**15** and oseltamivir during the 200 ns simulation

TABLE 3. *in silico* ADMET profile summary of compounds **11-15**

Parameter	Compound				
	11	**12**	**13**	**14**	**15**
Molecular weight (Da)	229.27	275.32	301.35	342.43	324.42
TPSA (Ã…Â²)	67.79	89.45	95.32	111.81	91.58
LogP	0.57	1.23	1.85	2.35	2.69
GI absorption	High	High	High	High	High
Solubility	Very Soluble	Soluble	Soluble	Soluble	Soluble
BBB permeability	No	No	No	No	No
P-gp substrate	No	No	No	Yes	No
CYP inhibition	No	No	No	No	No
Bioavailability score	0.55	0.55	0.55	0.55	0.55

profiles and show no PAINS alerts, supporting clean pharmacological profiles. The uniform bioavailability score of 0.55 suggests moderate oral absorption potential across the series.

CONCLUSIONS

In this study, we have successfully synthesized *tert*-butyl(1*S*,6*R*)-3-cyano-6-hydroxy-5-(pentan-3-yloxy) cyclohex-3-en-1-yl)carbamate **15** as the key intermediate of oseltamivir phosphate in 8 steps with an overall yield of 41%. In addition to the successful synthesis of compound **15**, computational evaluations provided essential insights into its potential as an antiviral agent. Molecular docking studies indicated that compound **15** exhibits strong binding affinity towards the neuraminidase enzyme, with interactions resembling those of oseltamivir. Molecular dynamics simulations further confirmed its stability within the active site, as shown by RMSD and RMSF analyses. The SwissADME evaluation established its favourable pharmacokinetic profile, highlighting its high oral bioavailability, solubility, and minimal metabolic liabilities. Importantly, the compound does not exhibit significant CYP inhibition, reducing the risk of drug-drug interactions.

ACKNOWLEDGEMENTS

The authors would like to acknowledge the financial support from Universiti Teknologi MARA Malaysia (600-RMC/LESTARI SDG-T 5/3 (164/2019). Supplementary data for synthesis of *tert*-butyl ((1*S*,6*R*)-3-cyano-6-hydroxy-5-(pentan-3-yloxy)cyclohex-3-en-yl)carbamate as key intermediate for oseltamivir phosphate is available from the corresponding author.

REFERENCES

Abrecht, S., Harrington, P., Iding, H., Karpf, M., Trussardi, R., Zutter, U. & Karpf, M. 2004. The synthetic development of the anti-influenza neuraminidase inhibitor oseltamivir phosphate (Tamiflu ®): A Challenge for Synthesis & Process Research. *CHIMIA* 58(9): 621-629.

Ali, M.T.M., Husin, Z.M. & Macabeo, A.P.G. 2021. Asymmetric synthesis of N,O-heterobicyclic octanes and (-)-Geissman-Waiss-Lactone. *ACS Omega* 6(38): 24614-24618.

Blanksby, S.J. & Ellison, G.B. 2003. Bond dissociation energies of organic molecules. *Accounts of Chemical Research* 36(4): 255-263.

Chen, C.A. & Fang, J.M. 2013. Synthesis of oseltamivir and tamiphosphor from N-acetyl-d-glucosamine. *Organic and Biomolecular Chemistry* 11(44): 7687-7699.

Cong, X. & Yao, Z.J. 2006. Ring-closing metathesis-based synthesis of (3R,4R,5S)-4-acetylamino-5- amino-3-hydroxy-cyclohex-1-ene-carboxylic acid ethyl ester: A functionalized cycloalkene skeleton of GS4104. *Journal of Organic Chemistry* 71(14): 5365-5368.

Davies, B.E. 2010. Pharmacokinetics of oseltamivir: An oral antiviral for the treatment and prophylaxis of influenza in diverse populations. *The Journal of Antimicrobial Chemotherapy* 65(2): ii5-ii10.

Hansen, K.B., Leighton, J.L. & Jacobsen, E.N. 1996. On the mechanism of asymmetric nucleophilic ring-opening of epoxides catalyzed by (salen) CrIII complexes. *Journal of the American Chemical Society* 118(44): 10924-10925.

Harrington, P.J., Brown, J.D., Foderaro, T. & Hughes, R.C. 2004. Research and development of a second-generation process for oseltamivir phosphate, prodrug for a neuraminidase inhibitor. *Organic Process Research and Development* 8(1): 86-91.

Ishikawa, H., Suzuki, T. & Hayashi, Y. 2009. High-yielding synthesis of the anti-influenza neuramidase inhibitor (−)-Oseltamivir by three "one-pot" operations. *Angewandte Chemie* 121(7): 1330-1333.

Karpf, M. & Trussardi, R. 2001. New azide-free transformation of epoxides into 1,2-diamino compounds: Synthesis of the anti-influenza neuraminidase inhibitor oseltamivir phosphate (Tamiflu). *Journal of Organic Chemistry* 66(6): 2044-2051.

Kim, C.U., Lew, W., Williams, M.A., Liu, H., Zhang, L., Swaminathan, S. & Stevens, R.C. 1997. Influenza neuraminidase inhibitors possessing a novel hydrophobic interaction in the enzyme active site: Design, synthesis, and structural analysis of carbocyclic sialic acid analogues with potent anti-influenza activity. *Journal of the American Chemical Society* 119(4): 681-690.

Kotsuki, H., Ohishi, T. & Araki, T. 1997. A new facile method for the chemoselective reductive transformation of azides to N-(tert-butoxycarbonyl) amines. *Tetrahedron Letters* 38(12): 2129-2132.

Martínez, L.E., Leighton, J.L., Carsten, D.H. & Jacobsen, E.N. 1995. Highly enantioselective ring opening of epoxides catalyzed by (salen)Cr(III) complexes. *Journal of the American Chemical Society* 117(21): 5897-5898.

Mita, T., Fukuda, N., Roca, F.X., Kanai, M. & Shibasaki, M. 2007. Second generation catalytic asymmetric synthesis of tamiflu: Allylic substitution route. *Organic Letters* 9(2): 259-262.

Murphy, E.F., Mallat, T. & Baiker, A. 2000. Allylic oxofunctionalization of cyclic olefins with homogeneous and heterogeneous catalysts. *Catalysis Today* 57(1-2): 115-126.

Perlman, N. & Albeck, A. 2000. Efficient and stereospecific synthesis of (Z)-hex-3-enedioic acid, a key intermediate for Gly-Gly cis olefin isostere. *Synthetic Communications* 30(24): 4443-4449.

Sagandira, C.R. & Watts, P. 2020. Continuous-flow synthesis of (-)-oseltamivir phosphate (Tamiflu). *Synlett* 31(19): 1925-1929.

Sagandira, C.R. & Watts, P. 2019. Efficient continuous flow synthesis of ethyl shikimate: The first step in the synthesis of Tamiflu. *Journal of Flow Chemistry* 9(2): 79-87.

Satoh, N., Akiba, T., Yokoshima, S. & Fukuyama, T. 2009. A practical synthesis of (-)-oseltamivir. *Tetrahedron* 65(16): 3239-3245.

Shibasaki, M., Kanai, M. & Yamatsugu, K. 2011. Recent development in synthetic strategies for oseltamivir phosphate. *Israel Journal of Chemistry* 51(3-4): 316-328.

Shie, J.J., Fang, J.M., Wang, S.Y., Tsai, K.C., Cheng, Y.S.E., Yang, A.S., Hsiao, S.C., Su, C.Y. & Wong, C.H. 2007. Synthesis of tamiflu and its phosphonate congeners possessing potent anti-influenza activity. *Journal of the American Chemical Society* 129(39): 11892-11893.

Singh, P., Gupta, E., & Mishra, N. 2020. Shikimic acid as intermediary model for the production of drugs effective against influenza virus. *Phytochemicals as Lead Compounds for New Drug Discovery* 2020: 245-256.

Trajkovic, M., Ferjancic, Z. & Saicic, R.N. 2011. An aldol approach to the enantioselective synthesis of (-)-oseltamivir phosphate. *Organic and Biomolecular Chemistry* 9(20): 6927-6929.

World Health Organization. 2016. *Influenza*. https://www.who.int/teams/health-product-policy-and-standards/standards-and-specifications/vaccines-quality/influenza

Yeung, Y.Y., Hong, S. & Corey, E.J. 2006. A short enantioselective pathway for the synthesis of the anti-influenza neuramidase inhibitor oseltamivir from 1,3-butadiene and acrylic acid. *Journal of the American Chemical Society* 128(19): 6310-6311.

Zhu, S., Yu, S., Wang, Y. & Ma, D. 2010. Organocatalytic Michael addition of aldehydes to protected 2-amino-1-nitroethenes: The practical syntheses of Oseltamivir (Tamiflu) and substituted 3-aminopyrrolidines. *Angewandte Chemie* 49(27): 4656-4660.

Zutter, U., Iding, H., Spurr, P. & Wirz, B. 2008. New efficient synthesis of oseltamivir phosphate (Tamiflu) via enzymatic desymmetrization of a meso-1,3-cyclohexanedicarboxylic acid diester. *Journal of Organic Chemistry* 73(13): 4895-4902.

*Corresponding author; email: tajudinali@uitm.edu.my